HEFAT2012
9th International Conference on Heat Transfer, Fluid Mechanics and Thermodynamics
16 – 18 July 2012
Malta

INSIGHT INTO THE UNSTEADY AERODYNAMICS OF FLOATING WIND TURBINES WITH TENSION LEG PLATFORMS (TLP) USING A BLADE ELEMENT MOMENTUM (BEM) BASED MODEL

Sean Agius.[1]* and Tonio Sant.[1]
*Author for correspondence
[1] Department of Mechanical Engineering,
University of Malta,
Msida MSD 2080,
Malta
E-mail: sagi0018@um.edu.mt

ABSTRACT

Floating wind turbines are subject to more complex dynamic behaviour than those mounted on fixed foundations. Such behaviour is dictated by the interaction of the hydrodynamic forces on the floater, the aerodynamic loads on the turbine as well as the gravitational and inertia loads.

Numerical simulation tools provide a valuable aid for obtaining further insight about the aerodynamics of floating wind turbines. A full-scale 5MW floating wind turbine model has been analyzed using a commercial numerical tool The unsteady aerodynamic effects were simulated using a BEM-based model modified to account for dynamic inflow effects.

Simulations under normal operation were conducted for a range of different wind speeds and tip speed ratios of the turbine rotor. One-directional water wave conditions were used in all simulations. Various parameters predicted by the simulation as a function of time where analyzed. These included the power output, power coefficient, and rotor axial thrust together with local blade parameters (including the angle of attack, velocities, lift and drag coefficients). Relationships were highlighted between the varied loading conditions. Furthermore, the results for the oscillating wind turbine were compared with those for the same turbine operating in a steady environment (i.e. with a rigidly fixed foundation).

NOMENCLATURE

c	[-]	Chord
f	[Hz]	Wave Frequency
k	[-]	Reduced Frequency
r/R	[-]	Fraction of Blade Radius
R	[m]	Blade Radius
C_D	[-]	Drag Coefficient
C_L	[-]	Lift Coefficient
C_P	[-]	Power Coefficient
$C_{P,i}$	[-]	Instantaneous Power Coefficient
C_T	[-]	Thrust Coefficient
$C_{T,i}$	[-]	Instantaneous Thrust Coefficient
2D		Two Dimension
3D		Three Dimension

Special characters

α	[^{0}]	Angle of Attack
λ	[-]	Tip Speed Ratio
λ_a	[-]	Average Tip Speed Ratio
λ_i	[-]	Instantaneous Tip Speed Ratio
Ω	[rpm]	Rotor Angular Velocity

INTRODUCTION

Given the important advantages it offers over existing wind energy technologies, floating offshore wind turbine technology has recently gained considerable interest [1], [2]. Floating technology enable wind turbines to be installed in deep water at sites farther away from the coast where wind conditions are superior and where permitting issues normally encountered in land-based and near-shore installations are not problematic. However, supporting an offshore turbine is, from an engineering design and economic point of view, more challenging given the fact that the turbine performance and lifetime are directly dependent on the dynamics of the floating platform itself.

Floating wind turbines are subject to more complex dynamic behaviour than those mounted on fixed foundations. Such behaviour is dictated by the interaction of the hydrodynamic forces on the floater, the aerodynamic loads on the turbine as well as the gravitational and inertia loads [3], [4], [5]. Hydrodynamic and inertial loads impart an oscillating behaviour of the structure, which in turn expose the rotor to a higher level of unsteady aerodynamics. Further knowledge is required to assess how the aerodynamics of wind turbines would be influenced by the motion of the floater under different operating wind and sea conditions. Having a detailed

understanding of these phenomena will lead to better performance techniques and more cost effective design solutions. It will also enable the development of more reliable control strategies to optimize rotor efficiency and minimize extreme and fatigue loads on the floating turbines.

To date, experimental data about to the aerodynamics of floating wind turbine rotors has been very limited. In these circumstances, numerical tools provide a valuable aid for obtaining further insight into the characteristics of floating wind turbines. The main goal of this paper was to provide a better understanding of the unsteady aerodynamics of a floating wind turbine using a commercial numerical tool code capable of modelling the unsteady behaviour. From an aerodynamic perspective, this analysis sheds more light on the behaviour of the output power and stall characteristics of the floating wind turbine. This study investigates also the influence of the rotor aerodynamic loads and tip speed ratio on the surge motion of the floating platform. In addition, the simulated results may be useful for planning future experimental campaigns on wind turbine aerodynamics.

FOATING WIND TURBINE SPECIFICATIONS

The floating wind turbine modelled was the full-scale MIT/NREL TLP structure fitted with the NREL 5-MW wind turbine system [6]. The primary objective of this conceptual floating wind turbine was to provide realistic and standardized input data required to assess the dynamics, loads and performance of offshore wind turbines in deep waters.

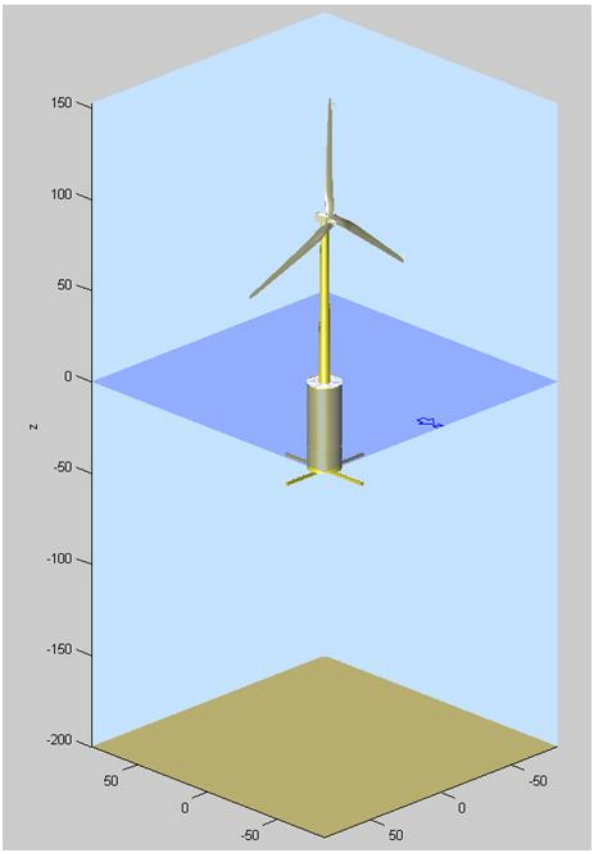

Figure 1 5MW MIT/NREL TLP as simulated in *Bladed*®.

The MIT/NREL TLP is a platform designed at the Massachusetts Institute of Technology (MIT) specifically to support the rotor, nacelle, and tower of the NREL baseline 5-MW system (see **Figure 1**). The resulting MIT/NREL TLP is a cylindrical platform, ballasted with concrete and moored by four pairs of vertical tendons in tension. Each pair of tendons is linked to a spoke that extends horizontally from the base of the platform. The main properties of the MIT/NREL TLP are summarized in **Table 1**. For further details about the TLP structure the reader is referred to [7], [6].

The U.S. Department of Energy's (DOE's) National Renewable Energy Laboratory (NREL), has developed the NREL offshore 5-MW baseline wind turbine. This is a large wind turbine that represents a typical utility-scale land- and sea-based multi-megawatt turbine. The NREL offshore 5-MW baseline wind turbine is based on the extensive design of the RePower 5M machine, and on the Dutch Offshore Wind Energy Converter (DOWEC) conceptual offshore wind turbine design and analysis project [8]. The model used in this study was derived from a composite of these data, summarized in **Table 2**. Additional information such as aerofoil and blade data can be found in [9], as well as in [6]. Data about the hydrodynamic properties, such as the drag and inertia coefficients of the platform, are available in [10].

Platform diameter	18 m
Platform draft	47.89 m
Water depth	200 m
Mooring system angle	90°
Concrete mass	8,216,000 kg
Platform Steel mass	378542 kg
Total displacement of water	12,187m^3
Number of mooring lines	8
Fairlead distance from center	18 m
Un-stretched mooring-line length	151.73 m
Line diameter	0.127
Line mass per unit length	116.03 kg/m
Line extensional stiffness	1,500,000,000 N

Table 1 Properties of MIT/TLP Platform.

Rating	5MW
Rotor Orientation, Configuration	Upwind, 3 Blades
Rotor, Hub Diameter	126 m, 3 m
Hub Height	90 m
Cut-In, Rated, Cut-Out Wind Speed	3 m/s, 11.4 m/s, 25 m/s
Cut-In, Rated Rotor Speed	6.9 rpm, 12.1 rpm
Rated Tip Speed	80 m/s
Overhang, Shaft Tilt, Precone	5 m, 5º, 2.5º
Rotor Mass	110,000 kg
Nacelle Mass	240,000 kg
Tower Mass	347,460 kg
Coordinate Location of Overall Center of Mass	(-0.2 m, 0.0 m, 64.0 m)

Table 2 Properties for the NREL 5-MW Baseline Wind Turbine.

BEM-BASED MODEL DESCRIPTION

Having established the floating wind turbine model, the next step was to input its properties to the software. This section provides a brief description of the selected numerical tool, *Bladed® v.4.1*, developed by Garrad Hassan™.

Bladed® is a design tool that has been extensively validated using a wide range of turbines. It has been certified by Germanischer Lloyd. This design code enables users to conduct the full range of performance and loading calculations [11].

Bladed® is a Blade Element Momentum (BEM) based model modified to account for tip and root loses and dynamic inflow effects [12]. The model also includes a development of the Beddoes dynamic stall sub-model to correct for unsteady and yawed phenomena. These sub-models are essential in this analysis because the floating platform motion causes the relative wind speed seen by the blades to become unsteady. Because *Bladed*® does not have a stall delay model, the 2D aerofoil data provided are pre-corrected for 3D effects. The software is also capable of modelling a varying wind field in both a spatial and time domain, taking into account wind shear and turbulence. *Bladed*® also is able to model different types of sea waves and current states. Waves are modelled by linear Airy theory and stream function theory for extreme wave conditions. Waves and currents are converted to forces, applied on the structure, by Morison's equation. The code also embeds a structural module for modelling the structural dynamic behaviour of the system, including the aero-elastic effects experienced by the turbine's blades. However, this paper is concerned solely with the analysis of the aerodynamics of the wind turbine on the moving platform and assumes a rigid floating wind turbine. Consequently, the structural module was not used. For further details about the software *Bladed*®, the reader is referred to [12].

All the necessary MIT/NREL TLP specifications were inputted into *Bladed*® and simulations under normal operation throughout a range of wind and water wave conditions were undertaken. Different tip speed ratios for the turbine rotor were taken into account. In all the simulations carried out, it was assumed that the structure, primarily the tower and blades, were rigid. Hence, the effect of blade aero-elasticity was ignored. To simplify the study, only operational scenarios with one dimensional sea waves were investigated. The presence of sea currents and tides was also ignored.

NUMERICAL SIMULATIONS

Initial numerical simulations were carried out in order to validate the wind turbine input specifications. For the same wind turbine and load specifications, results outputted by *Bladed*® and the ones simulated by NREL [6], gave realistically good agreement.

Following the validation procedure, simulations were designed and implemented to expose the physical phenomena that take place in a floating wind turbine. The TLP structure was subjected to a combination of wind and wave load cases. Wind speeds were maintained constant in both spatial and temporal domain. Also, the wind front was maintained uniform, with no presence of shear, yaw and turbulence. However, the rotor angular velocity was varied to be able to study the effect of the tip speed ratio on the floating structure's response. Moreover, probable and realistic Mediterranean wave scenarios were selected from [13]. These waves are summarized in **Table 3**.

Wave frequency (Hz)	***Wave height (m)***	***Wave period (s)***
0.222	0.7	4.5
0.182	1.9	5.5
0.118	4.9	8.5

Table 3 Wave Parameters

These different load cases allow various parameters to be analyzed as a function of time. These included the power output, power coefficient, rotor axial thrust together with local blade parameters (including the angle of attack, lift and drag coefficients). Furthermore, simulations for the same turbine, but operating in a steady environment (i.e. with a rigidly fixed foundation) were also undertaken. Essentially this served to highlight the difference in the output parameters for a fixed turbine and a floating one.

It is important to note that the simulation time inputted in the *Bladed*® code for each load case was long enough to enable the structure to reach the steady state, thereby eliminating the transient state in the analysis.

RESULTS & ANALYSIS

Previous results show that when a floating wind turbine is subjected to wind and waves the structure will oscillate about a mean position. To confirm these results and to analyse the response of a real multi-megawatt wind turbine with six modes of motion, the forthcoming simulations were performed. A constant wind speed of 10 m/s and waves of different heights and periods (as per **Table 3**) were generated. These were set to be directed to the rotor, with no presence of yaw and wind/wave misalignment. The direction of the wind and waves is displayed in **Figure 1** by the arrow.

It was observed that the TLP has a relatively large movement in the surge mode (movement parallel to wind and wave direction), when compared to other translational and rotational modes of motion. Results also showed that very small side to side deflections are experienced. The resulting surge motions by the MIT/NREL TLP for 0.118 Hz and for 0 Hz wave frequencies are given in **Figure 2** and **Figure 3** respectively. It should be noted that f = 0 Hz is not implying that the turbine is rigidly fixed to the ground, but that the floating wind turbine is not subjected to sea waves. It may be observed that the TLP undergoes an oscillatory (sinusoidal) movement due to the hydrodynamic force produced by the waves. At no wave conditions the oscillations are very small, having an order of a few centimetres. These very small disturbances are due to the endless interaction between two forces: the buoyancy force, which is trying to restore the TLP to its original position and the thrust force generated by the rotor due to the wind. The effect of the tip speed ratio as well

as the wave frequency on the surge displacement will be discussed later on.

Oscillation of the TLP structure causes the structure to experience a relative oscillating velocity. As the structure moves back and forth into the wind, the rotor experiences a high flow speed in the forward direction and a low flow speed in the backward direction. Assuming rigid blades, these are exposed to a velocity field composed of the wind speed and the structure's oscillating velocity. In all the simulations conducted the angular velocity of the rotor was maintained constant with time. Consequently, the velocity diagram at the blade element and the resulting angle of attack depend on the velocity acting on the blade. Hence, the fluctuation in the velocity leads to a fluctuation in the angle of attack. This causes the rotor to work in an unsteady environment, thus showing the importance of using a dynamic stall model. **Figure 2** illustrates the variation in the angle of attack with time, discussed above, for a wave frequency of 0.118 Hz at different tip speed ratios, while **Figure 4** illustrates variation in the angle of attack for 0 Hz wave frequency (i.e. no wave condition). A comparison of **Figure 4** with **Figure 3** shows that the frequency of oscillation of the angle of attack at $\lambda = 3$ with no wave condition is four times that of the surge oscillation. Thus, it can be concluded that the angle of attack oscillation cannot be attributed to the surge oscillation. At $\lambda = 3$ the rotor's angular velocity is 4.5 rpm. Examining **Figure 4** one can note that in 60 seconds there are approximately 4.5 wave periods. Because the rotor is slightly tilted upwards (by 5^0, see **Table 2**), a difference in the incoming velocity across the azimuth angle is experienced, which in turn leads to a variation of the angle of attack. This concludes that the oscillation of the angle of attack is due to the tilt of the rotor. However, comparing **Figure 5** with **Figure 2** one can see that the angle of attack's oscillation frequency at $\lambda = 3$ is identical to that of the surge. The oscillation resulting from the rotor tilt is significantly smaller than that resulting from the platform surge. This produces an irregular fluctuation of the angle of attack with time (**Figure 5**), which is in contrast with the smaller sinusoidal wave produced by the tilted rotor alone (**Figure 4**). The resulting fluctuations in the lift coefficient may be found in **Figure 6**.

Figure 7to **10**, illustrate in greater detail the degree of unsteadiness a blade of a floating turbine on a TLP is exposed to due to fluctuation in the angle of attack at the individual blade sections. The loops shown in **Figure 7** evidently display the present of dynamic stall phenomenon. For the outboard region (r/R = 0.8) and at f = 0 Hz the mean angle of attack predicted by the code is approximately 18.5^0 with a variation of $\pm 1^0$whereas for the inboard region (r/R = 0.3) the mean angle of attack is approximately 32.5^0 with a variation of $\pm 2.5^0$. Hence, at the inboard region the aerofoil is stalled and has larger fluctuating amplitude compared with the outboard region. The above conforms to the rotor reduced frequency (k) equation which is given by:

$$k = \frac{Mc}{2R}$$

Flow is said to be an unsteady one when $k > 0.05$ [14], where M is a constant. The reduced frequency is increased as the radius decreases (going from outboard to inboard region) as shown by the above equation. The unsteadiness of the flow increases with a higher reduced frequency. This can be confirmed by **Figure 7**. The circle-like loops indicate that the angle of attack is varying with a sinusoidal fashion. For the wave frequency of 0.118 Hz these circle loops are not defined well. Furthermore, the mean and range angle of attacks are larger than that f = 0 Hz. This proves that in a wave dominated scenario the degree of unsteadiness is increased considerably. A superimposition of the static aerofoil data is also shown on **Figure 7**. **Figure 8** displays the blade section aerofoils operating in attached flow at $\lambda = 12$. Here, the unsteadiness is highly reduced. As expected, the mean and associated variation in the angle of attack at the inboard region is larger than those at the outboard regions.

The fluctuation experienced by the angle of attack and the lift coefficient will naturally cause a fluctuation in the output power as well as the thrust of the turbine rotor. **Figure 11** and **Figure 12** show how the power and thrust vary with time between a mean position; this mean position being the output power of a fixed turbine. This power fluctuation leads to loss of power quality, which needs to be handled by appropriate control systems. One should take note that the turbine is operating at a lower rated velocity, therefore it is not producing the rated 5MW of power.

To analyse the effect of the floating turbine's dynamics and the power coefficient of the turbine, C_P vs. λ curves for different wave conditions were plotted. The relative velocity across the rotor changes continuously as the platform is subjected to waves. Because the power coefficient and tip speed ratio depend on this relative velocity, both will change continuously with time. Plots of instantaneous power coefficient and tip speed ratio for different wave frequencies are plotted in **Figure 13** and **Figure 14**. The simulated complex unsteady behaviour resulted in clouds of data points in these graphs. The mean, maximum and minimum of the fluctuated power coefficient are incorporated in these plots. It is evident that for all wave frequencies the deviation between the maximum and minimum power coefficient (i.e. the power coefficient fluctuation) increases as the tip speed ratio increases (**Figure 17**). This phenomenon was also seen during measurements on a scaled wind turbine installed on TLP platform in a wind/wave generator facility at the University of Malta [15].

An analysis was carried out with *Bladed*® to compare the mean output power from a wind turbine installed on a floating turbine with that generated when the same turbine is rigidly fixed at its base. The result of this analysis is seen in **Figure 18.** The predicted results indicate that under different wave frequencies there is no loss in the mean power coefficient as a result of the floater motion. It can be concluded that both floating and fixed turbines can generate the same average power, irrespective of the wave frequency. This may also be observed from **Figure 19** and **Figure 20**. However, measurements on scaled wind turbine at the University of Malta have actually reported a small decrease in average power coefficient when the same turbine was installed on a floater [15] .

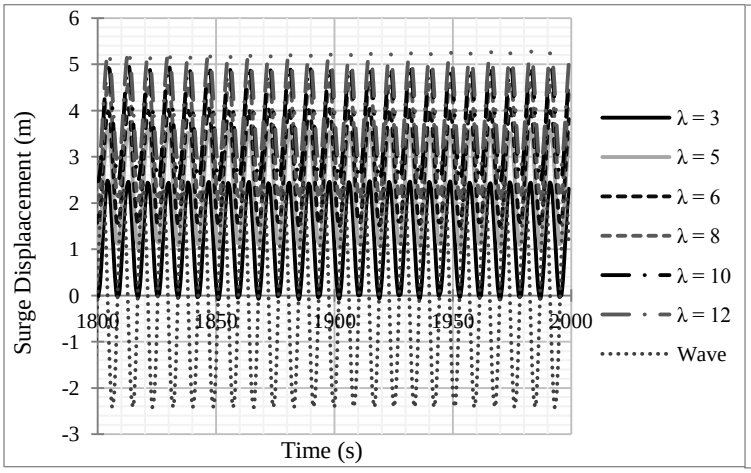

Figure 2 Surge Displacement vs. Time at f = 0.118 Hz for different λ.

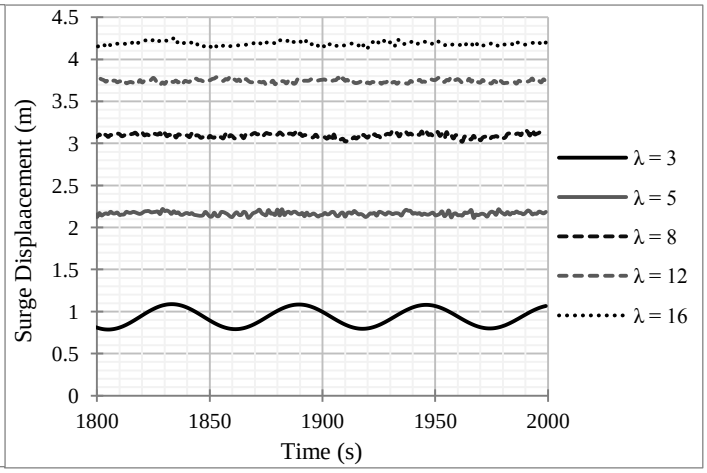

Figure 3 Surge Displacement vs. Time at f = 0 Hz for different λ.

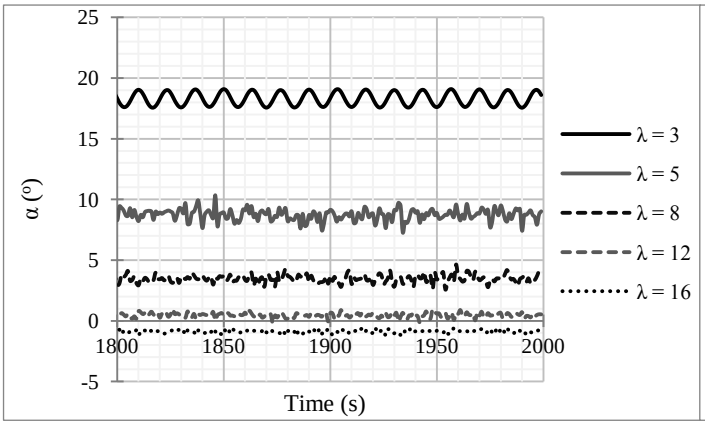

Figure 4 Angle of attack at a r/R = 0.8 blade location vs. Time at f = 0 Hz & for different λ.

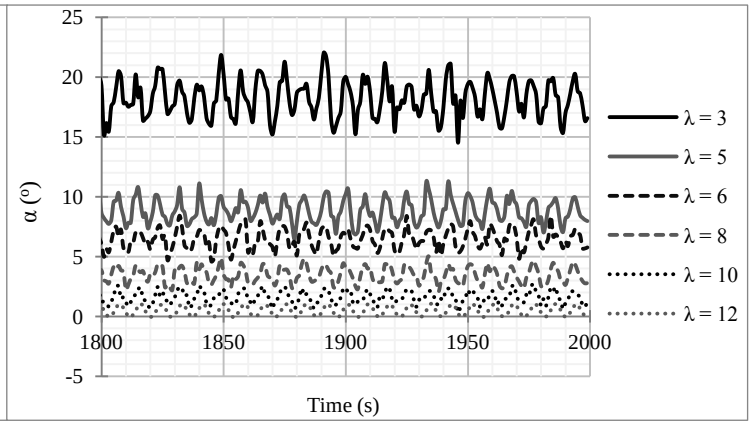

Figure 5 Angle of attack at a r/R = 0.8 blade location vs. Time at f = 0.118 Hz & for different λ.

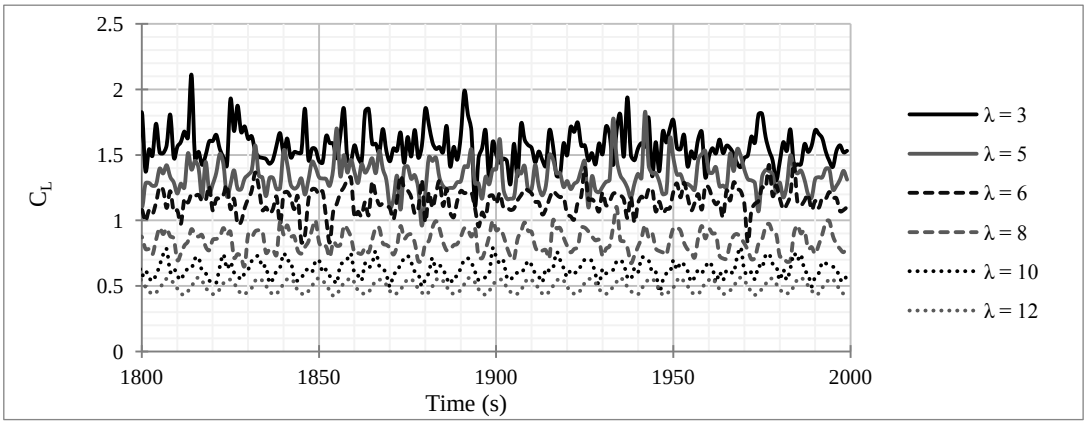

Figure 6 Lift Coefficient at a r/R = 0.8 blade location vs. Time at f = 0.118 Hz & for different λ.

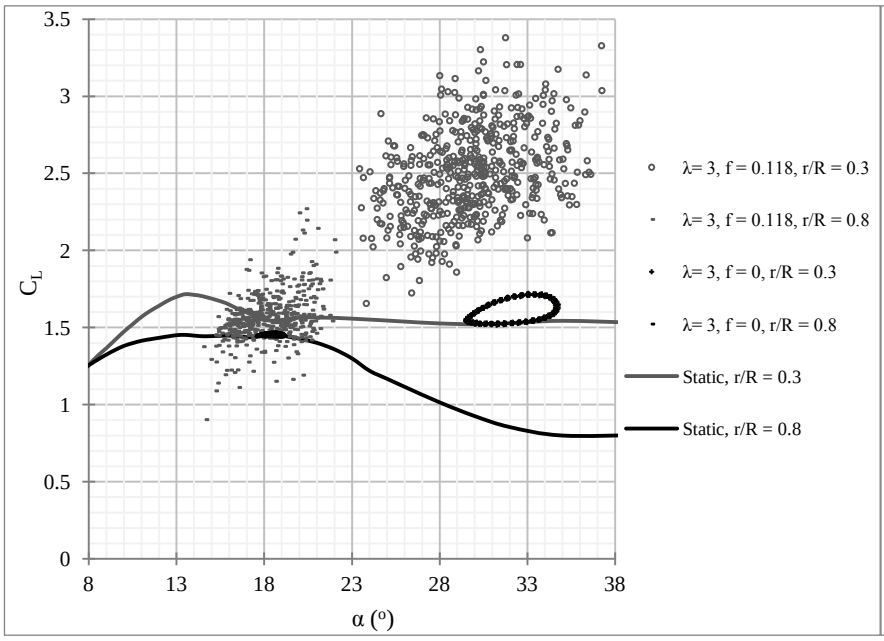

Figure 7 Dynamic Lift Coefficient vs. Angle of attack at λ = 3 for different r/R sections and wave conditions.

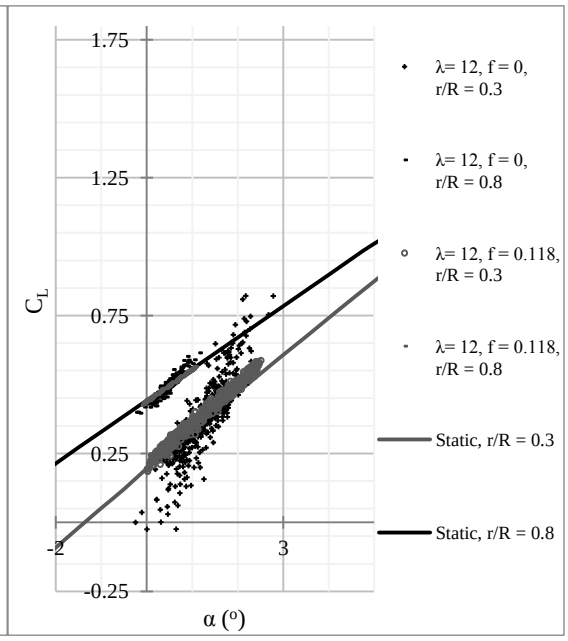

Figure 8 Dynamic Lift Coefficient vs. Angle of attack at λ = 12 for different r/R sections and wave conditions.

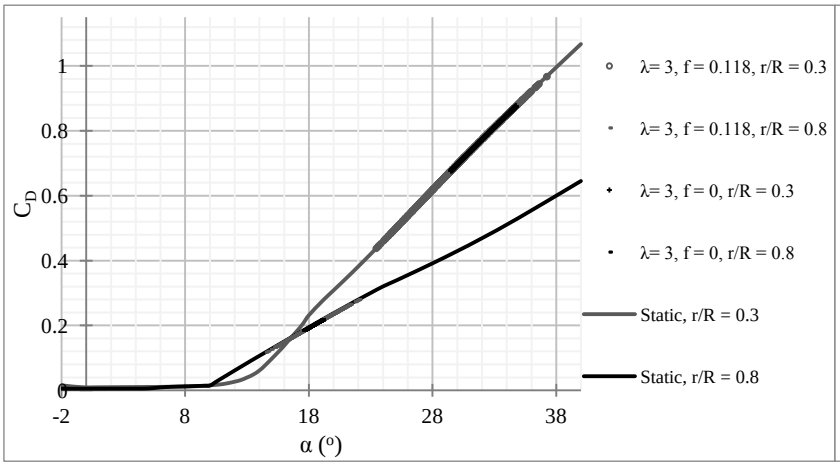

Figure 9 Dynamic Drag Coefficient vs. Angle of attack at λ = 3 for different r/R sections and wave conditions.

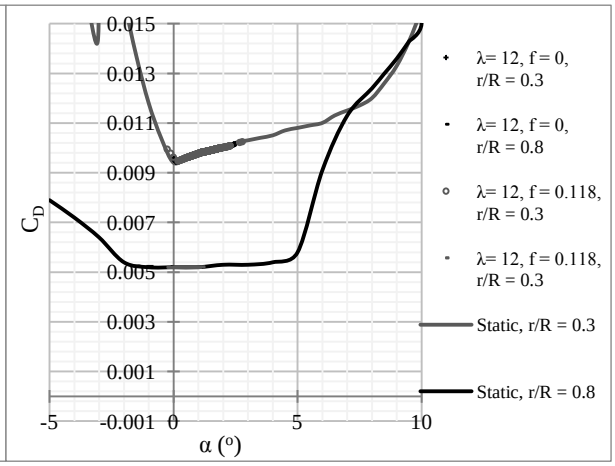

Figure 10 Dynamic Drag Coefficient vs. Angle of attack at λ = 12 for different r/R sections and wave conditions.

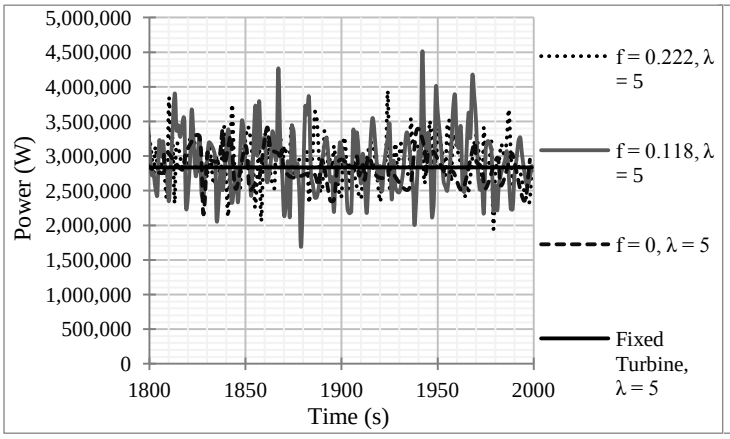

Figure 11 Power vs. Time at λ = 5 for different wave conditions.

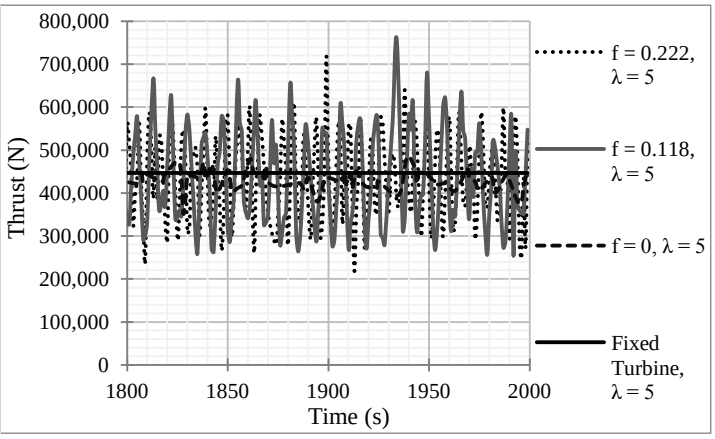

Figure 12 Thrust vs. Time at λ = 5 for different wave conditions.

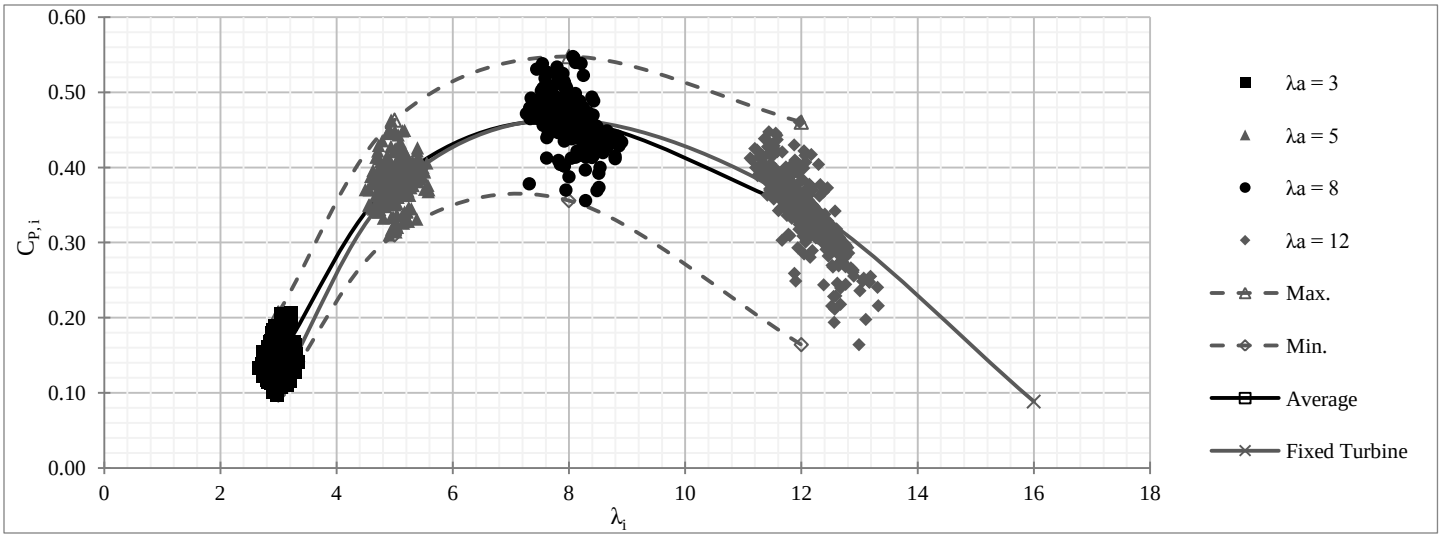

Figure 13 Instantaneous Power Coefficient vs. Instantaneous Tip Speed Ratio at f = 0.182 Hz.

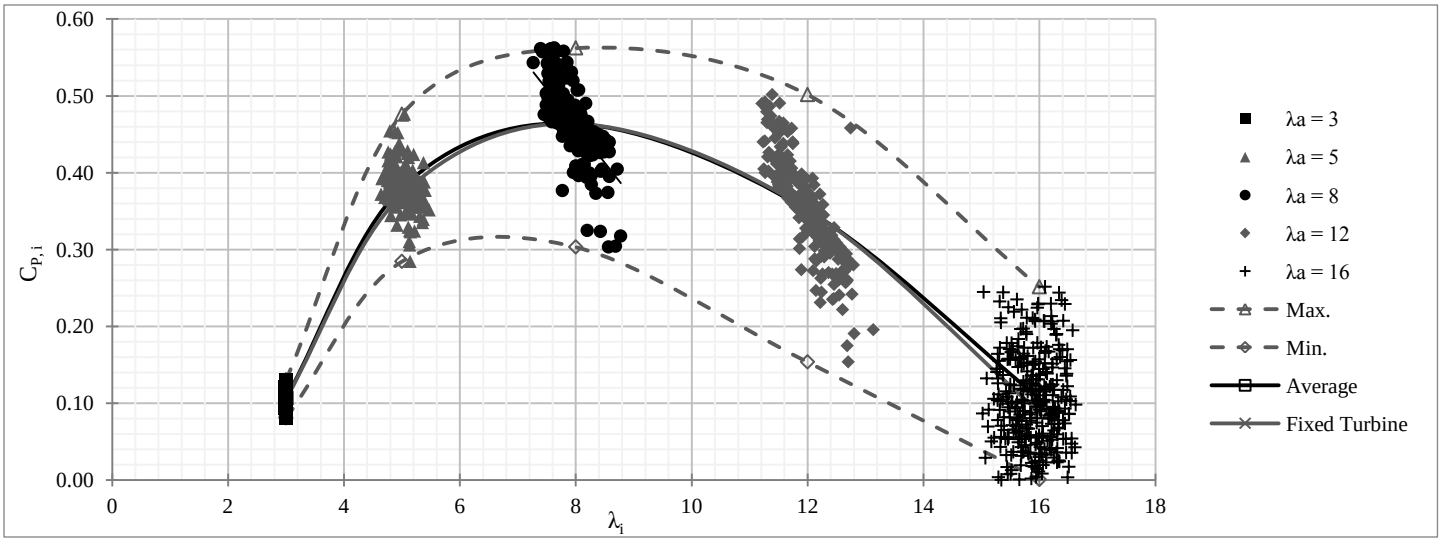

Figure 14 Instantaneous Power Coefficient vs. Instantaneous Tip Speed Ratio at f = 0 Hz.

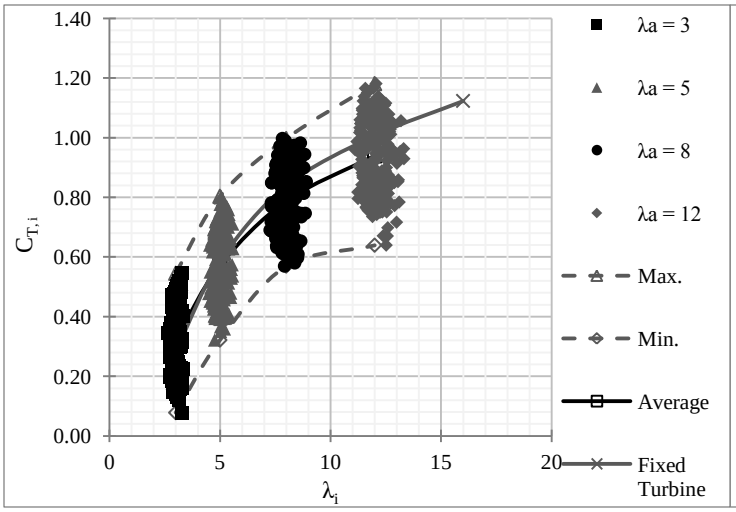

Figure 15 Instantaneous Thrust Coefficient vs. Instantaneous Tip Speed Ratio at f = 0.182 Hz.

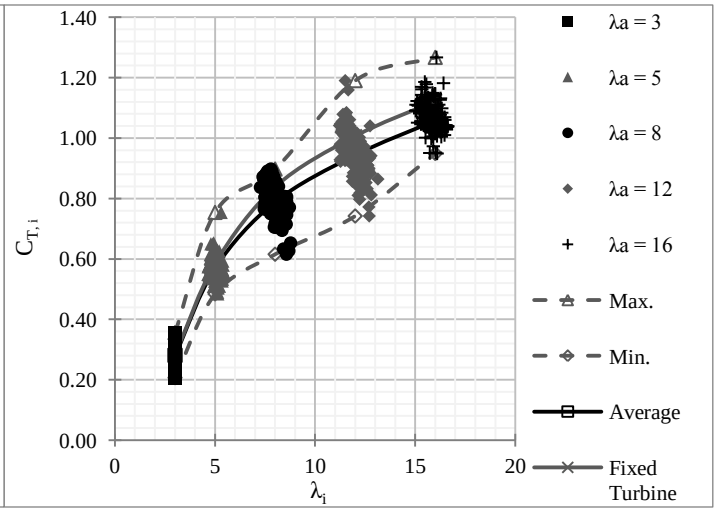

Figure 16 Instantaneous Thrust Coefficient vs. Instantaneous Tip Speed Ratio at f = 0 Hz.

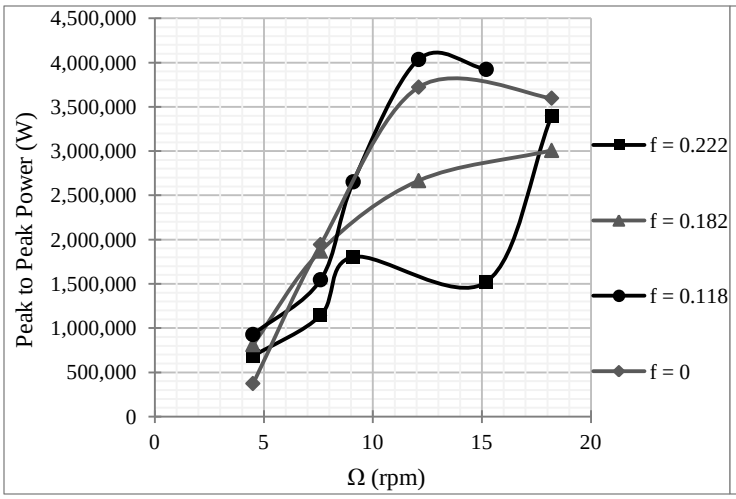

Figure 17 Peak to Peak Power vs. Rotor Angular Velocity at different wave conditions.

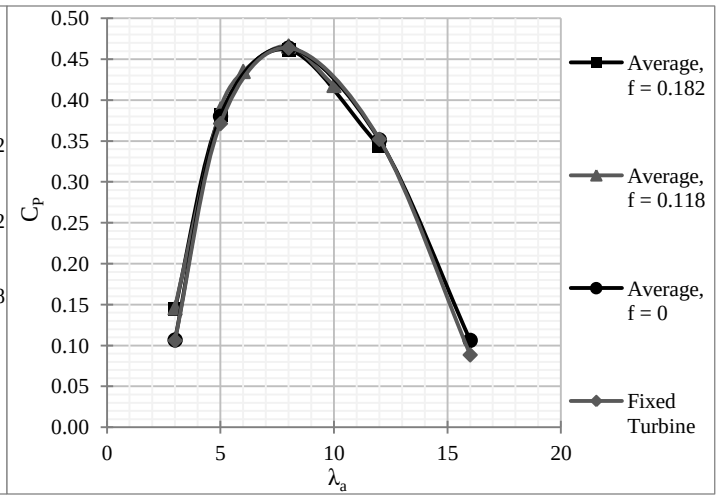

Figure 18 Power Coefficient vs. Average Tip Speed Ratio at different wave conditions.

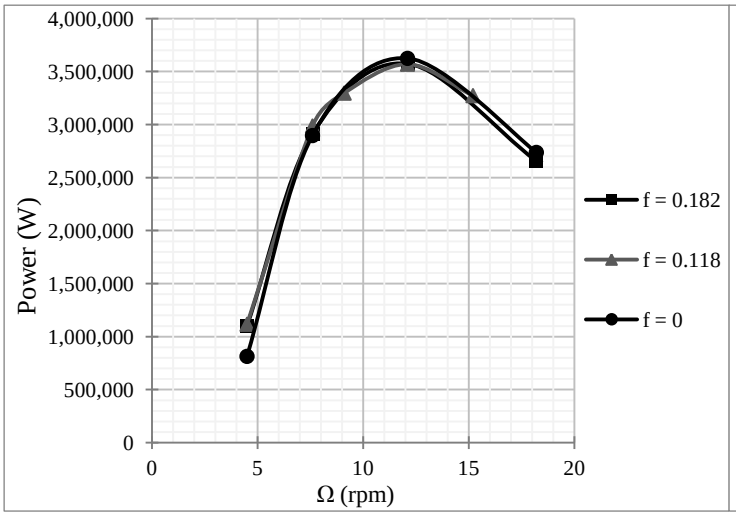

Figure 19 Mean Power Generated vs. Rotor Angular Velocity at different wave conditions.

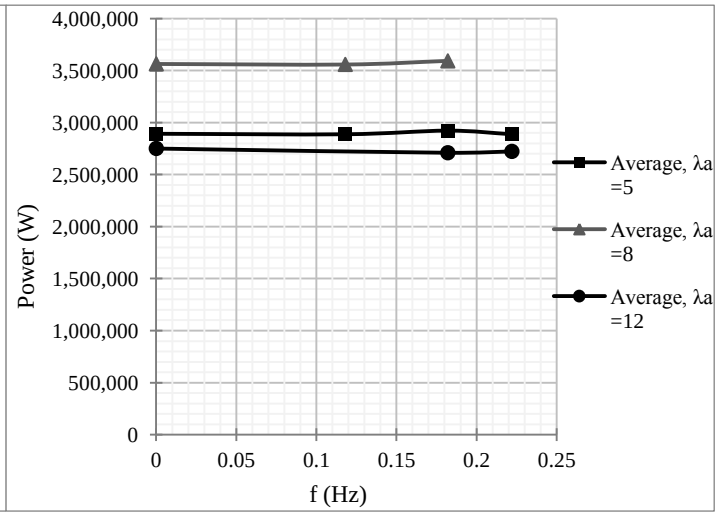

Figure 20 Power Generated vs. Wave Frequency at different at different tip speed ratios.

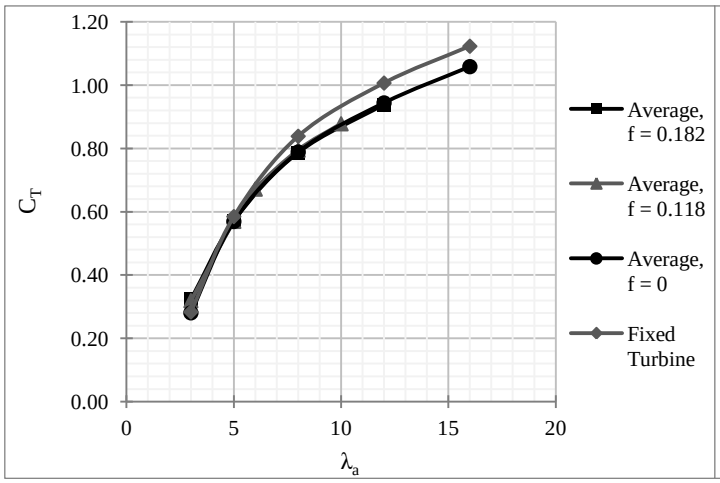

Figure 21 Thrust Coefficient vs. Average Tip Speed Ratio at different wave conditions.

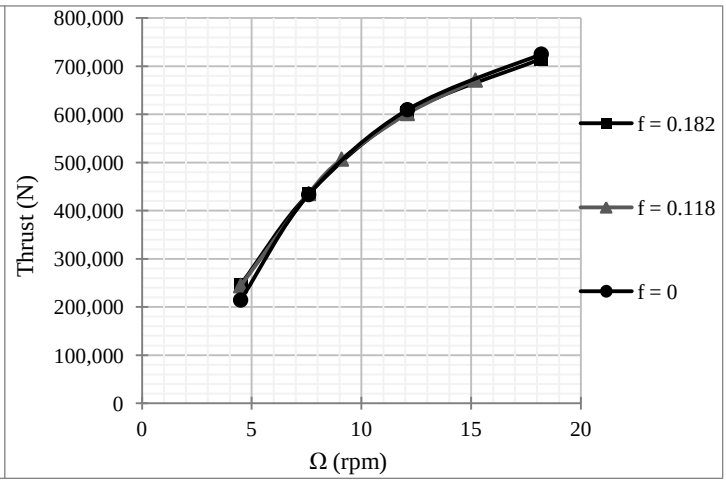

Figure 22 Mean Thrust vs. Rotor Angular Velocity at different wave conditions.

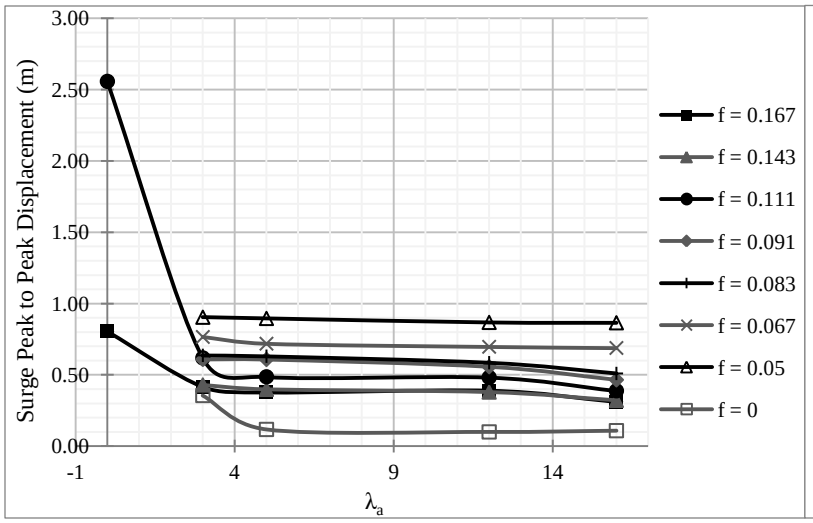

Figure 23 Surge Peak to Peak Displacement vs. Average Tip Speed Ratio at different wave conditions.

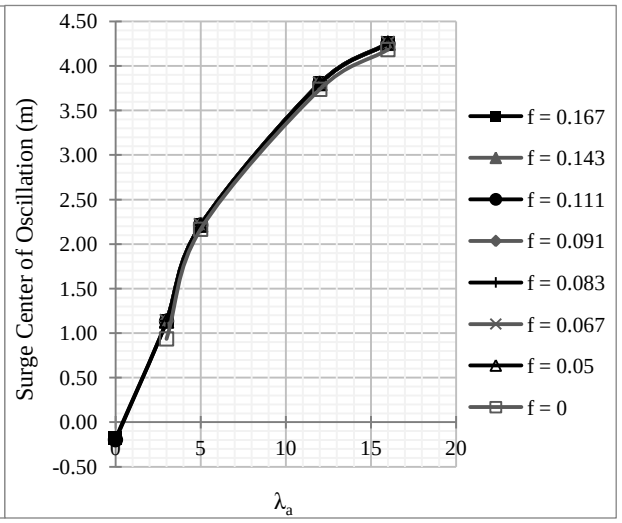

Figure 24 Surge Centre of Oscillation vs. Average Tip Speed Ratio at different wave conditions.

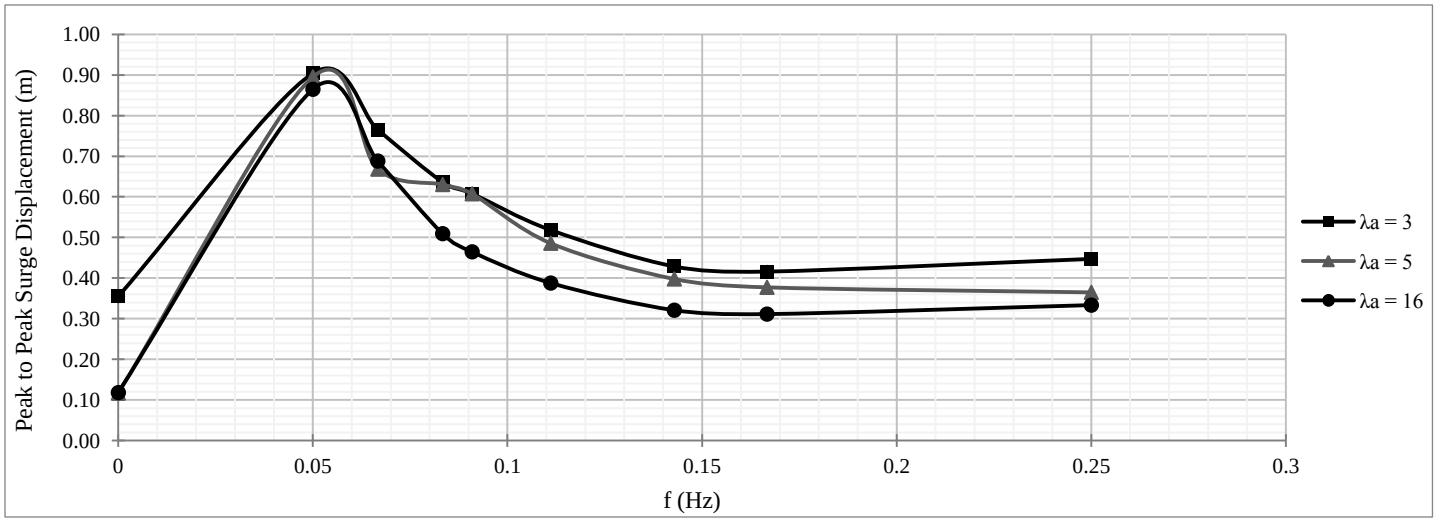

Figure 25 Surge Peak to Peak Displacement vs. Wave Frequency at different tip speed ratios.

Figure 15 and **Figure 16** display the cloud of data points for the instantaneous thrust coefficient with the instantaneous tip speed ratio. Also shown are the maximum, minimum and average thrust coefficients. These graphs confirm that increasing the tip speed ratio increases the thrust fluctuation as shown earlier for the power coefficient. The average thrust coefficient of different wave frequencies was compared with the thrust coefficient generated by the fixed wind turbine. **Figure 21** is predicting a lower thrust coefficient for the floating wind turbine as compared with that for a fixed turbine. This is true for all wave frequencies analysed. The thrust as a function of the rotor angular velocity is shown in **Figure 22**. For a constant wind the thrust experienced by the rotor increases as the angular velocity increases.

The peak to peak surge distance (the maximum to minimum distance of oscillation) was plotted as a function of tip speed ratio for several of wave frequencies (see **Figure 23)**. High peak to peak displacements occur at low tip speed ratios, particularly at $\lambda = 0$ (rotor switched off).

The peak to peak displacement decreases as the tip speed ratio increases until it becomes nearly constant. This is due to the presence of aerodynamic damping, where in fact the thrust force on the rotor acts as an aerodynamic damper. **Figure 23** illustrates an interesting phenomenon, where the peak to peak surge displacement decreases as the wave frequency increases. From **Figure 24** it is shown that as the tip speed ratio increases so does the centre of oscillation. This means that the centre of oscillation moves further downwind. This downwind movement is attributed to the large thrust of the rotor as the tip speed ratio increases, (**Figure 21**). This effect is being predicted to be nearly independent of wave frequency.

In **Figure 25** the effect of the peak to peak surge displacement as a function of wave frequency and different tip speed ratios is displayed. When the wave frequency increases from zero, the peak to peak surge displacement increases consistently until it reaches a maximum at approximately 0.055 Hz. At higher frequencies, the peak to peak starts to decay until it reaches a constant value. This behaviour is due to the

structure's dynamic response of the floating system. It can be concluded that the natural frequency of the TLP is between 0.04 Hz and 0.06 Hz. Therefore, it is expected that operating at this frequency range the TLP structure is subjected to a higher fatigue. In addition as the tip speed ratio is increased the peak to peak decreases. This is attributed to the increment of thrust with the tip speed ratio, thereby providing higher aerodynamic damping.

CONCLUSION

The 5MW MIT/NREL TLP was simulated under different rotor tip speed ratios and different one-dimensional wave conditions using the commercially available design code, *Bladed*®.

The surge displacement, power and thrust coefficient, angle of attack, lift and drag coefficients for the floating turbine were modelled. This study provided more insight on how the motion and performance parameters of the floating wind turbine fluctuate under the effect of wave motion.

This surge motion was observed to be dependent on the wave frequency and tip speed ratio. It was seen that as the tip speed ratio increases the aerodynamic damping increases which in turn reduces the surge peak to peak motion. As the wave frequency increases from the natural frequency of the turbine/TLP structure, the peak to peak surge displacement also decreases. This results in lower fatigue, especially in the moorings.

In this analysis it was demonstrated that the rotor of a floating wind turbine is dominated by unsteady flow, even though the wind speed was maintained constant. Consequently, the angle of attack, lift and drag coefficients are subjected to oscillations. In turn these parameters affect the loads seen by the blade and thus higher fatigue loads are experienced, mainly at the blade roots.

The power and thrust coefficient of the turbine subjected to wave action deviated considerably from that simulated by a fixed wind turbine (i.e. no structure movement). The deviations were more pronounced at higher tip speed ratios. Unlike a turbine on a rigid base, a floating turbine experiences considerable fluctuations in the output power. However the model predicted an average power coefficient of a floating wind turbine to be very similar to that produced by a fixed turbine. From an economic point of view this is a very important result, since the floating turbine will generate the same power for the same rotor speed and wind conditions.

REFERENCES

[1] European Wind Energy Association , "Wind in our Sails - The coming of Europe's offshore wind energy industry," European Wind Energy Association, EWEA Report 2011.

[2] Ocean Energy Council, "Offshore Wind Energy," Ocean Energy Council, Florida, Information about Ocean Renewable Energy Report.

[3] T. Sebastian and M. A. Lackner, "Offshore Floating Wind Turbines - An Aerodynamic Perspective," University of Massachusetts, Massachusetts, Research Report.

[4] J. M. Jonkman, "Dynamics Modeling and Loads Analysis of an Offshore Floating Wind Turbine," National Renewable Energy Laboratory, Technical Report 2007.

[5] J. E. Withee, "Fully Coupled Dynamic Analysis of a Floating Wind Turbine System," Massachusetts Institute of Technology, Doctoral Thesis 2004.

[6] J. Jonkman and T. Fischer, "Model Development and Loads Analysis of an Offshore Wind Turbine on a Tension Leg Platform, with comparision to other Floating Turbine Concepts," National Renewable Energy Laboratory , U.S., 2009.

[7] J. Jonkman and D. Matha, "A Quantitative Comparison of the Responses of Three Floating Platforms," National Renewable Energy Laboratry, Conference Paper 2010.

[8] H. J. T. Kooijman, C. Lindenburg, D. Winkelaar, and E. L. van der Hooft, "Aero-elastic modelling of the DOWEC 6 MW pre-design in PHATAS," Technical Report 2003.

[9] J. Jonkman, S. Butterfield, and W. Musial, "Definition of a 5-MW Reference Wind Turbine for Offshore System Development," National Renewable Energy Laboratory, Technical Report 2009.

[10] G. K.V. Ramachandran, H. Bredmose, J. N. Sorensen, and J. J. Jensen, "Response of a TLP Floating Wind Turbine subjected to combined Wind and Wave Loading," Dept. of Mechanical Eng., Technical University of Denmark, Denmark,.

[11] GL Garrad Hassan. GL Group-Bladed. [Online]. http://www.gl-garradhassan.com/en/GHBladed.php

[12] Garrad Hassan and Partners Ltd , "Bladed Theory Manual v.4.1," Garrad Hassan and Partners Ltd., Bristol, Theory Manual 2010.

[13] BMT ARGOSS. Wave Climate. [Online]. http://www.waveclimate.com/

[14] J. Gordon Leishman, *Principles of Helicopter Aerodynamics*. Cambridge, UK: Cambridge University Press, 2000.

[15] D. Bonnici, S. Agius, T. Sant, and D. Micallef, "Motion and Performance Analysis of An Experimental Model Floating Wind Turbine," Department of Mechanical Engineering, University of Malta, Malta, EWEA Offshore 2011 Paper 2011.